Nanoscale

Cite this: *Nanoscale*, 2012, **4**, 5431

www.rsc.org/nanoscale

PAPER

Hierarchically plasmonic photocatalysts of Ag/AgCl nanocrystals coupled with single-crystalline WO_3 nanoplates†

Deliang Chen,*[ab] Tao Li,[a] Qianqian Chen,[a] Jiabing Gao,[a] Bingbing Fan,[a] Jian Li,[a] Xinjian Li,[b] Rui Zhang,[ac] Jing Sun[d] and Lian Gao[d]

Received 28th April 2012, Accepted 28th May 2012
DOI: 10.1039/c2nr31030a

The hierarchical photocatalysts of Ag/AgCl@plate–WO_3 have been synthesized by anchoring Ag/AgCl nanocrystals on the surfaces of single-crystalline WO_3 nanoplates that were obtained *via* an intercalation and topochemical approach. The heterogeneous precipitation process of the PVP–Ag^+–WO_3 suspensions with a Cl^- solution added drop-wise was developed to synthesize AgCl@WO_3 composites, which were then photoreduced to form Ag/AgCl@WO_3 nanostructures *in situ*. WO_3 nanocrystals with various shapes (*i.e.*, nanoplates, nanorods, and nanoparticles) were used as the substrates to synthesize Ag/AgCl@WO_3 photocatalysts, and the effects of the WO_3 contents and photoreduction times on their visible-light-driven photocatalytic performance were investigated. The techniques of TEM, SEM, XPS, EDS, XRD, N_2 adsorption–desorption and UV-vis DR spectra were used to characterize the compositions, phases and microstructures of the samples. The RhB aqueous solutions were used as the model system to estimate the photocatalytic performance of the as-obtained Ag/AgCl@WO_3 nanostructures under visible light ($\lambda \geq 420$ nm) and sunlight. The results indicated that the hierarchical Ag/AgCl@plate–WO_3 photocatalyst has a higher photodegradation rate than Ag/AgCl, AgCl, AgCl@WO_3 and TiO_2 (P25). The contents and morphologies of the WO_3 substrates in the Ag/AgCl@plate–WO_3 photocatalysts have important effects on their photocatalytic performance. The related mechanisms for the enhancement in visible-light-driven photodegradation of RhB molecules were analyzed.

Introduction

Environmental purification and energy conversion on the basis of highly efficient photocatalysts and solar energy attract more and more attention.[1] As a typical photocatalyst, TiO_2 nanocrystals have been extensively studied, but the large energy band gaps restrict their wide applications in visible-light or sunlight.[2,3] Seeking new photocatalysts with suitable energy gaps or modifying TiO_2 with various doping elements (*i.e.*, S, N, Fe, *etc.*) has been a hot topic in recent decades.[4–6] In the most recent years, the surface plasmon resonance (SPR) of metal nanoparticles has been introduced to photocatalysts, because of the enhanced absorption in the visible light region.[7–9] The typical plasmonic photocatalysts include (Ag,Au)/TiO_2,[9–12] Ag/AgX (X = Cl, Br, I),[13–19] Ag/C[20] and their analogous systems.

Constructing hierarchical nanostructures for photocatalytic applications by anchoring functional species on semiconductors or even insulators is a novel strategy to improve their performance.[21–23] For plasmonic photocatalysts, there are a number of reports on hierarchical nanostructures, including Ag_3PO_4/TiO_2,[24] Ag/AgBr/TiO_2,[25–29] Ag/AgX/GO (X = Cl, Br),[30,31] AgX/Ag_3PO_4 (X = Cl, Br, I),[32] $Ag_8W_4O_{16}$/AgCl,[33] AgI/AgCl/TiO_2,[34] Ag–AgI/Fe_3O_4@SiO_2,[35] Ag/AgBr/BiOBr[36] and Ag–AgI/Al_2O_3.[37]

For Ag/AgCl plasmonic photocatalysts, Long *et al.*[38] developed Ag–AgCl/$BiVO_4$ photocatalysts for MO (10 mg L^{-1}, in ~60 min, $\lambda \geq 400$ nm) photodegradation, and claimed that O_2^- is the main active species in the degradation reaction. Dai *et al.*[39] precipitated Ag/AgCl on P25 to synthesize Ag/AgCl/TiO_2 photocatalysts for visible-light-driven photoreduction of Cr(VI) and organic dyes. An *et al.*[40] reported a magnetic visible-light-driven plasmonic Fe_3O_4@SiO_2@AgCl:Ag photocatalyst. Quan *et al.*[41] reported Ag@AgCl/RGO hybrid photocatalysts. Other systems,

[a]*School of Materials Science and Engineering, Zhengzhou University, 100 Science Road, Zhengzhou 450001, P.R. China. E-mail: dlchen@zzu.edu.cn; Fax: +86-371-67781593; Tel: +86-371-67781046*
[b]*School of Physics and Engineering, Zhengzhou University, 100 Science Road, Zhengzhou 450001, P.R. China*
[c]*Aeronautical Industry Management, University Centre, Zhengdong New District, Zhengzhou 450046, P.R. China*
[d]*The State Key Laboratory of High Performance Ceramics and Superfine Microstructure, Shanghai Institute of Ceramics, Chinese Academy of Sciences, Shanghai 200050, China*

† Electronic supplementary information (ESI) available: The schematic of the synthesis of Ag/AgCl@plate–WO_3 photocatalysts; a summary of the synthetic parameters and photodegradation rate constants of the Ag/AgCl@WO_3 photocatalysts and some other samples for the purposes of comparative investigation. See DOI: 10.1039/c2nr31030a

including Ag/AgCl/ZnO,[42] Ag/AgCl/BiOCl,[43] Ag/AgCl/titanate honeycomb,[44] Ag/AgCl/TNT,[45] and Ag/AgCl/polyacrylonitrile fibers,[46] have also been investigated. These hierarchically composite photocatalysts usually take on enhanced performance in many cases when compared with their separate compositions, but the well-controlled substrates on a larger scale are not available.

Tungsten oxide (WO_3) is generally more positive (+0.5 V *vs.* NHE) than the reduction potentials of O_2 due to the deeply positive level of the band value (mainly consisting of O 2p orbitals), which makes WO_3 unsuitable for achieving the efficient oxidative decomposition of organic compounds in air.[6] WO_3 is seldom studied as a photocatalyst for the oxidative decomposition of organic compounds,[47] but WO_3-based nanostructures can be used as substrates to construct composite photocatalysts, such as AgBr/WO_3,[48] AgBr/H_2WO_4,[49] Ag/AgBr/$WO_3 \cdot H_2O$,[50] and Ag/AgCl/$W_{18}O_{49}$ or Ag/AgCl/WO_3.[51] However, the morphologies of these WO_3 or $WO_3 \cdot H2O$ nanostructures are not well controlled, and their influencing effects on the photocatalytic performance are not clear.

We recently developed an efficient and robust method to synthesize WO_3 nanoplates on the basis of intercalation and topochemical conversion.[52–55] The as-obtained WO_3 nanoplates are of a high diameter-to-thickness ratio and single-crystalline structure, having a specific surface area larger than 150 $m^2\ g^{-1}$.[54] This kind of two-dimensional WO_3 nanoplate is suitable as an efficient substrate to design hierarchical composite photocatalysts. In addition, we developed a sonochemical route to synthesize Ag/AgCl nanocubes with unique photodegradation performance for organic dyes under visible-light irradiation.[56]

We here present a hierarchically plasmonic photocatalyst of Ag/AgCl@plate–WO_3 by anchoring Ag/AgCl nanoparticles on the surfaces of ultrathin, single-crystalline WO_3 nanoplates for the first time. The WO_3 nanoplates with small thicknesses (~10 nm) and high specific surface areas were used as the substrates. The Ag/AgCl nanoparticles with a size of ~100 nm were formed *in situ* through a precipitation reaction, followed by a photoreduction process. Other WO_3 powders with various morphologies (*i.e.*, nanorods and nanoparticulates) were also used as the substrates to fabricate Ag/AgCl@WO_3 photocatalysts for a comparative study. The compositions, microstructures and photocatalytic properties of the as-obtained hierarchical photocatalysts were carefully investigated. The effects of the contents of WO_3 nanoplates, photoreduction times and the morphologies of the WO_3 substrates on the photocatalytic performance of the Ag/AgCl@WO_3 photocatalysts were studied. The possible mechanisms for the formation of photocatalysts and their enhanced photocatalytic properties were investigated.

Experimental

Materials

Tungsten trioxide (WO_3, analytically pure), tungstic acid (H_2WO_4, analytically pure), *n*-octylamine (chemically pure), polyvinylpyrrolidone K30 (PVP), and ammonium metatungstate ($(NH_4)_6H_2W_{12}O_{40} \cdot xH_2O$, analytically pure) were purchased from Sinopharm Chemical Reagent Co. Ltd. Silver nitride ($AgNO_3$, analytically pure) and heptane (analytically pure) were purchased from Tianjing Kermel Chemical Reagent Co. Ltd. Sodium chloride (NaCl, analytically pure) and hydrochloric acid (HCl, 36 wt%, analytically pure) were purchased from Luoyang Chemical Reagent Plant. Ethanol (analytically pure) was purchased from Anhui Ante Biochemical Co., Ltd. All the reagents were used as received without further purification. Distilled water was used in the experiments unless otherwise specifically stated.

Synthesis of ultrathin single-crystalline WO_3 nanoplates

WO_3 nanoplates were synthesized using an intercalation-topochemical approach according to our previous reports with some modification.[52,54] Typically, tungstic acid (18 g, 72 mmol) was dispersed in a mixture of *n*-octylamine (60 mL) and heptane (480 mL) at room temperature, and kept magnetically stirring for 72 h. A milky colloid was finally formed. The solid species were collected by filtration, washed using ethanol several times, and then air-dried at room temperature. The as-obtained product was tungstate-based inorganic–organic hybrids, which was used as the starting material for the synthesis of the WO_3 nanoplates. The as-obtained tungstate-based inorganic–organic hybrids (10 g) ware dispersed in an HNO_3 aqueous solution (~3 mol L^{-1}, 500 mL), and magnetically stirred for 48 h. The yellowish solid species were collected by filtration, washed with water and ethanol, and dried at 120 °C. The dried product was H_2WO_4 nanoplates. The as-obtained H_2WO_4 nanoplates were calcined at 500 °C for 1 h to form WO_3 nanoplates with a similar morphology. The as-obtained WO_3 nanoplates were then used as the substrate to fabricate Ag/AgCl@plate–WO_3 composite photocatalysts.

Synthesis of hierarchical Ag/AgCl@WO_3 composite photocatalysts

The Ag/AgCl@WO_3 composite photocatalysts were synthesized *via* a two-step approach, including a heterogeneous precipitation of AgCl nanocrystals on the WO_3 nanoplates, followed by a photoreducing reaction to form *in situ* a small amount of Ag species on the AgCl nanoparticles (Fig. S1, ESI†). Typically, 1.0 mmol of $AgNO_3$ was added to a water (30 mL)/ethanol (50 mL) mixture, containing 200 mg of WO_3 nanoplates and 0.111 g of PVP under magnetic stirring; then a Cl^- aqueous solution (20 mL) containing 0.5 mmol of NaCl and 0.086 mL of HCl aq. solution (36 wt%) was added drop-wise into the above WO_3–Ag^+ mixture (pH ≈ 2), and kept magnetically stirring for 24 h in the dark. The as-obtained milky suspension was then irradiated for 5 min using a 300 W Xe lamp with an ultraviolet cut-off filter (UV-cut 420) and turned darker and darker in color. The solid species were finally collected by centrifugation, and washed three times using water and ethanol, respectively. The above solid was then dried at 50 °C and used as a photocatalyst, which was marked as AA200pW5. Various amounts of WO_3 nanoplates and various photoreduction times were used to synthesize a series of Ag/AgCl@WO_3 composite photocatalysts under the same conditions. The details of these samples are listed in Table S1, ESI†.

For the purposes of comparison, WO_3 nanocrystals with other morphologies, *i.e.*, hydrothermal WO_3 nanorods and commercially available WO_3 nanoparticles, were also used to synthesize Ag/AgCl@WO_3 composite photocatalysts under similar conditions, and the samples were marked as AA200rW5 and AA200cW5, respectively (see Table S1, ESI†). The WO_3 nanorods were synthesized by hydrothermally treating a 0.1 mol L^{-1} ammonium metatungstate aqueous solution with a pH value of 2 (adjusted using HNO_3) at 180 °C for 24 h.

Characterization of compositions and microstructures

The phase compositions of the Ag/AgCl@WO_3 samples were determined by X-ray diffraction (XRD) performed on an XD-3 X-ray diffractometer (Beijing Purkinje General Instrument Co., Ltd., China) with Cu K_α irradiation (λ = 0.15406 nm). The morphologies and microstructures of the samples were observed using a field-emission electron scanning microscope (FE-SEM, JEOL 7500F), and a field-emission transmission electron microscope (FE-TEM, Tecnai G2 F20, accelerating voltage of 200 kV, Philips) with an attachment of energy dispersive analysis of X-rays (EDAX). The X-ray photoelectron spectroscopy (XPS) spectra were recorded on a multi purpose X-ray photoelectron spectroscope (Sigma Probe, Thermo VG Scientific) with a micro-focused monochromatic X-ray source (Al K_α), using adventitious carbon (C 1s = 284.6 eV) as the calibration reference. The UV-vis diffuse reflectance (DR) spectra were recorded on a Perkin-Elmer spectrometer (Lambda 950, Walthan, MA) in a wavelength range of 250–800 nm. The Brunauer–Emmett–Teller (BET) N_2 adsorption analysis was conducted on an ASAP 2020 physisorption analyzer (USA) with a pretreating temperature of 200 °C.

Measurement of photocatalytic activity

The photocatalytic properties of the as-obtained Ag/AgCl@WO_3 samples were tested using a home-made system equipped with an Xe lamp (NBeT, HSX-UV300) and an ultraviolet cut-off filter (UV-cut 420), providing a visible-light source ($\lambda \geq 420$ nm). The aqueous solutions of Rhodamine B (RhB) and methyl orange (MO) were used as the target pollutants to evaluate the visible-light-driven photocatalytic performance of these samples. All the experiments were conducted in ambient conditions. Typically, 30 mg of photocatalysts were firstly dispersed in a 100 mL beaker with a diameter of 60 mm, containing 30 mL of 10 mg L^{-1} RhB (or MO) aq. solutions under magnetic stirring in the dark. The distance between the bottom surface of the Xe lamp and the top surface of the beaker was kept at a constant of 160 mm. The above suspensions with dye molecules were kept stirring in the dark for 30 min to reach an adsorption–desorption equilibrium of dye molecules on the photocatalysts. Then, the suspensions with photocatalysts and dye molecules were exposed to the visible light irradiation. Aliquots of solutions (3 mL) were drawn out from the reaction system at given degradation durations (*i.e.*, 1 min). The suspensions sampled were centrifuged twice at 10 000 rpm for 10 min to separate the solid photocatalyst particles completely, and the top transparent solutions obtained were then transferred to a quartz cuvette to measure their absorption spectra in a wavelength range of 250–800 nm. The relative concentrations (C/C_0) of the RhB and MO aq. solutions were determined by the absorbance (A/A_0) at 554 nm and 464 nm, respectively, because of the relationship of $C = k'A$. Here, k' is a constant, A is the absorbance of the dye aqueous solution at time t and A_0 is the absorbance at the beginning of the visible-light irradiation. Similarly, C is the concentration of the dye aqueous solution at time t, and C_0 is the concentration at the beginning of the visible-light irradiation. For the photocatalytic experiments using sunlight, the conducting parameters were the same as those under visible light irradiation.

Results and discussion

Phases, compositions, morphologies and photocatalytic properties of typical hierarchical Ag/AgCl@plate–WO_3 nanostructures

Fig. 1 shows the typical XRD patterns of WO_3 nanoplates, Ag/AgCl nanoparticles and their composite species of Ag/AgCl@plate–WO_3 (AA200pW5) obtained by photo-reducing AgCl@plate-WO_3 for 5 min. As Fig. 1a shows, the WO_3 nanoplates, synthesized *via* the route of intercalation and topochemical conversion, can be indexed to a triclinic WO_3 phase (space group: $P\bar{1}$ [1]) according to the JCPDS card no. 32-1395.[55] The Ag/AgCl sample, obtained by photo-reducing AgCl in UV-visible light for 5 min, shows three major diffraction peaks at 28.06°, 32.48° and 46.54° in the 2θ range of 20–50°, which can be indexed to the

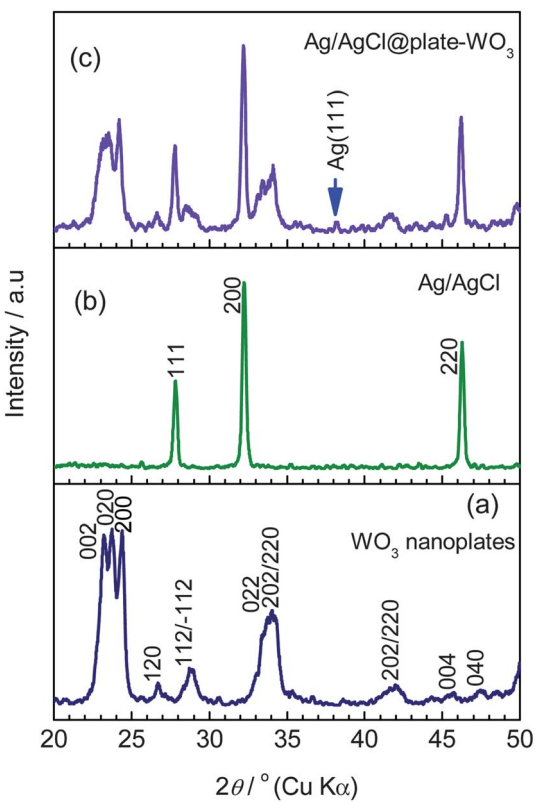

Fig. 1 Typical XRD patterns of (a) WO_3 nanoplates, (b) Ag/AgCl nanoparticles and (c) their composite photocatalyst of Ag/AgCl@plate–WO_3 (AA200pW5).

(111), (200) and (220) reflections of a cubic silver chloride phase (space group: *Fm*3*m* [225]) according to the JCPDS card no. 31-1238. The XRD pattern of the Ag/AgCl@plate–WO_3 (AA200pW5) sample, as shown as Fig. 1c, can be seen as the superimposition of the XRD patterns of WO_3 nanoplates and Ag/AgCl nanoparticles. Though the photoreduction conditions are the same (irradiation for 5 min under visible light), the Ag/AgCl sample does not show any obvious reflections belonging to metal Ag species, while the Ag/AgCl@plate–WO_3 sample shows a recognizable reflection at $2\theta \sim 38.1°$ (marked with an arrow in Fig. 1c) belonging to the metal Ag species in their XRD patterns. The possible explanation is that the amount of the Ag species photo-induced is too small to detect by the XRD method for the Ag/AgCl sample, and some similar results can be found in recent references.[56] For the Ag/AgCl@plate–WO_3 sample, WO_3 nanoplates, having a smaller band energy gap than that of AgCl,[54,57] can absorb more visible light ($\lambda \geq 420$ nm), which photogenerates more electrons to improve the photoreduction reaction.

Typical FE-SEM and TEM observations of the WO_3 nanoplates and Ag/AgCl@plate–WO_3 nanostructures are shown in Fig. 2. As Fig. 2a–c show, the WO_3 nanoplates of large surface areas ($\geq$120 m^2 g^{-1}) and small thicknesses ($\sim$10 nm) are single-crystalline, and these plate-like particles are loosely assembled into a typical "house-of-cards" structure, which effectively overcomes the agglomeration of nanocrystals and then provides large surface areas toward outer environments. The FE-SEM image of Ag/AgCl@plate–WO_3 nanostructures is shown in Fig. 2d, which indicates that the Ag/AgCl nanoparticles are uniformly anchored on the surfaces of the WO_3 nanoplates.

The TEM image of the Ag/AgCl@plate–WO_3 sample in Fig. 2e confirms that the AgCl nanoparticles are firmly attached on the surfaces of the WO_3 nanoplates. The corresponding EDS spectrum (Fig. 2f) obtained in the TEM observation shows that the Ag/AgCl@plate–WO_3 sample consists of W, Ag, O, and Cl as the major elements. The element Cu belongs to the C-coated Cu grid used in the TEM observation, and the element C comes from the C-coated Cu grid and the organic PVP molecules adsorbed on the Ag/AgCl@plate–WO_3 sample. It should be noted that the Ag-to-Cl ratio obtained from the EDS measurement in the TEM observation is not the actual composition because the AgCl species is so sensitive to electrons that most of the AgCl species are transformed to metal Ag species while the Cl species are released upon exposure to the electron beam.[56] From the SEM and TEM observations, one can confirm that the zero-dimensional Ag/AgCl nanoparticles are uniformly anchored onto the surfaces of the two-dimensional WO_3 nanoplates, forming a hierarchical Ag/AgCl@plate–WO_3 nanostructure with profuse outer surfaces and interfaces. This hierarchical nanostructure is especially favorable for photocatalytic applications because of not only the high surface areas, but also the enhanced stability of the loosely assembled functional nanocrystals.

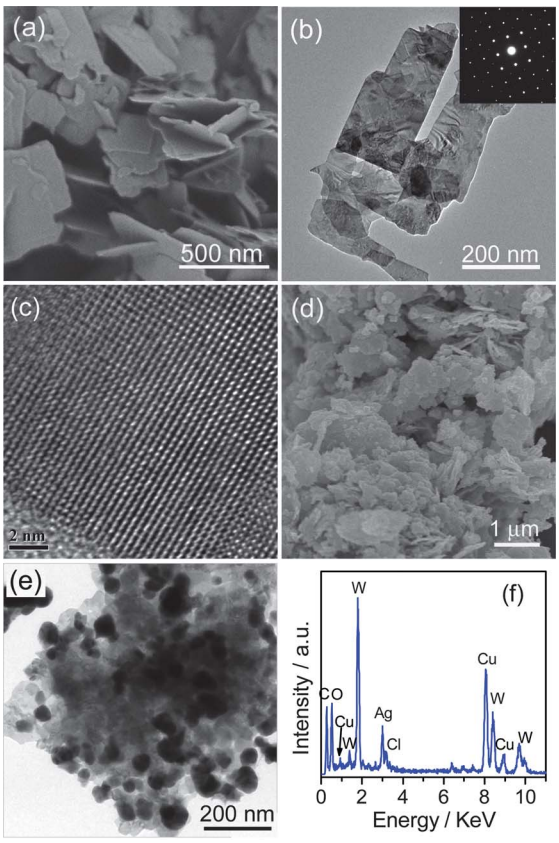

Fig. 2 (a) FE-SEM, (b) TEM and (c) HRTEM images of WO_3 nanoplates obtained *via* the intercalation and topochemical conversion process; (d) FE-SEM image, (e) TEM image and (f) EDS spectrum of the Ag/AgCl@plate–WO_3 (AA200pW5) photocatalyst obtained using WO_3 nanoplates as substrates.

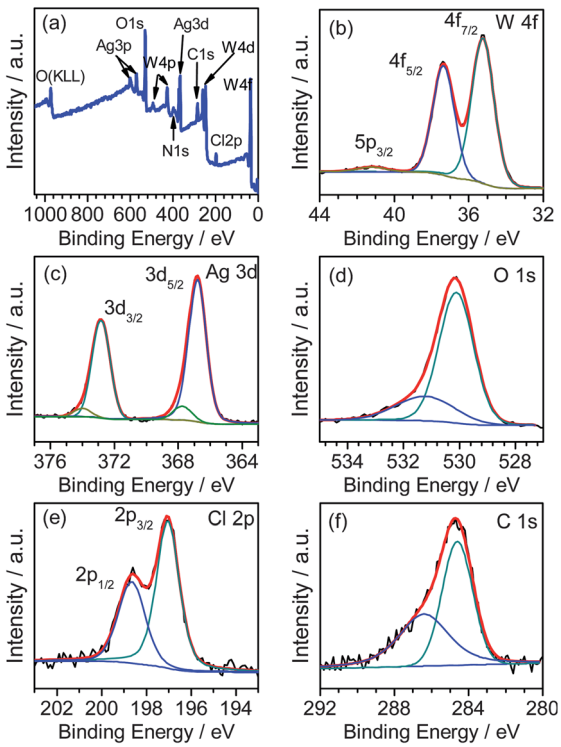

Fig. 3 Typical XPS spectra of the Ag/AgCl@plate–WO_3 (AA200pW5) photocatalyst: (a) a wide survey scan, (b) W 4f & 5p, (c) Ag 3d, (d) O 1s, (e) Cl 2p and (f) C 1s.

The chemical compositions of the hierarchical Ag/AgCl@plate–WO_3 nanostructures with a 5 min photoreducing reaction were characterized by XPS spectra, as shown in Fig. 3. The survey-scan spectrum in Fig. 3a indicates that the sample consists mainly of the elements W, Ag, O, Cl and C, besides a small amount of N. According to the synthetic and measuring processes, the peak of N 1s indicates that there is a trace amount of PVP molecules adsorbed on the surfaces of the Ag/AgCl@plate–WO_3 sample; the obvious C 1s peak mainly belongs to the PVP molecules and the carbon tape used to attach the sample powders during the XPS measurement; the W, Ag, O and Cl should belong to the Ag/AgCl@plate–WO_3 sample. The W 4f spectrum shown in Fig. 3b has two obvious peaks at 35.2 and 37.4 eV, belonging to W $4f_{7/2}$ and W $4f_{5/2}$ of WO_3, respectively. Fig. 3c shows the Ag 3d spectrum, which consists of two sets of peaks: one is the strong set with two peaks at 372.8 and 366.8 eV, which corresponds to the binding energies of Ag $3d_{3/2}$ and Ag $3d_{5/2}$ of AgCl, respectively; the other is the weak one with two peaks at 373.8 and 367.8 eV, which should be attributed to the binding energies of Ag $3d_{3/2}$ and Ag $3d_{5/2}$ of metal Ag, respectively.[30,31,36] The XPS results of Ag 3d confirm the existence of metal Ag species, agreeing with the XRD result (Fig. 1c). The molar ratio of metal Ag species to total Ag can be calculated to be ~27% according to the heights of the Ag $3d_{5/2}$ peaks. The O 1s spectrum in Fig. 3d can be well fitted by two peaks centered at 530.1 and 531.3 eV, which should belong to the WO_3 and PVP molecules, respectively. Fig. 3e shows two peaks at ~198.7 eV and ~197.0 eV, belonging to the Cl $2p_{1/2}$ and Cl $2p_{3/2}$ spectra of AgCl, respectively, with a doublet separation of 1.7 eV. Fig. 3f shows the high-resolution scan of C 1s, of which the weak peak with a binding energy of 286.4 eV belongs to the adsorbed PVP molecules and the strong peak at 284.6 eV should belong to the inorganic C from the carbon tape. The XPS spectra re-confirm that the hierarchical Ag/AgCl@plate–WO_3 nanostructures consist of WO_3, AgCl and metal Ag, besides a small amount of adsorbed PVP molecules.

The sunlight-driven photodegradation performance of the Ag/AgCl@plate–WO_3 nanostructures was also examined, and the typical results are shown in Fig. 4e and f. One can find that the RhB aq. solution can be decomposed completely in 18 min under sunlight (Fig. 4e). The corresponding $\ln(A/A_0) \sim t$ plot has a good linearity (Fig. 4f), indicating that the sunlight-driven photodegradation of RhB aq. solutions in the presence of Ag/AgCl@plate–WO_3 also follows the first-order kinetics. The simulated rate constant (k) under sunlight is 0.150(7) min^{-1}, less than that (0.58(3) min^{-1}) under the home-made visible light. A possible reason for this could be that the energy intensity of sunlight is less than that of the home-made visible light.

Fig. 5 shows the recycling properties of the hierarchical Ag/AgCl@plate–WO_3 photocatalyst for RhB aq. solutions under visible-light irradiation ($\lambda \geq 420$ nm). As the figure shows, the as-obtained Ag/AgCl@plate–WO_3 nanostructures show a fairly stable photocatalytic performance for RhB photodegradation. After a recycling application of three times, the photodegrading performance of the Ag/AgCl@plate–WO_3 photocatalyst slightly decreases, and its complete degradation time increases from 5 min for the first cycle to 8 min for the third one. The XRD pattern of the Ag/AgCl@plate–WO_3 sample after the recycling

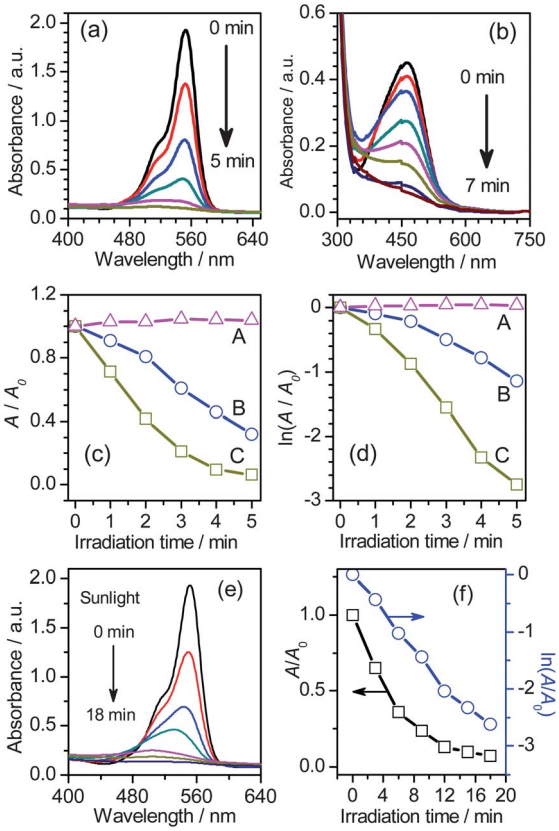

Fig. 4 Typical UV-vis spectral changes of (a) RhB and (b) MO aq. solutions (10 mg L^{-1}) in the presence of the Ag/AgCl@plate–WO_3 (AA200pW5) photocatalyst (1.0 g L^{-1}) under various visible-light ($\lambda \geq 420$ nm) irradiation times; (c) Plots of A/A_0 *vs.* the irradiation time for (A) RhB in the dark, (B) MO under visible light, and (C) RhB under visible light; (d) Plots of $\ln(A/A_0)$ *vs.* the irradiation time for (A) RhB in the dark, (B) MO under visible light, and (C) RhB under visible light; (e) The UV-vis spectra of RhB aq. solutions (10 mg L^{-1}) in the presence of the Ag/AgCl@plate–WO_3 (AA200pW5) photocatalyst (1.0 g L^{-1}) under sunlight light at various irradiation times, and (f) the corresponding plots of A/A_0 and $\ln(A/A_0)$ *vs.* the irradiation time.

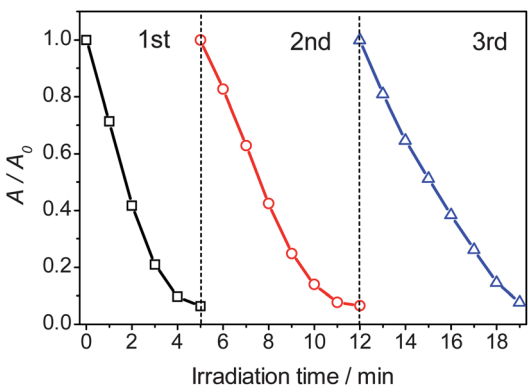

Fig. 5 Recycling properties of the as-obtained Ag/AgCl@plate–WO_3 (AA200pW5) photocatalyst for the photodegradation of RhB aq. solutions under visible-light irradiation ($\lambda \geq 420$ nm).

use indicates that the Ag content slightly increases but the major phases are still the AgCl and WO_3 phases (Fig. S2, ESI†). The morphology of the Ag/AgCl@plate–WO_3 photocatalyst before and after the RhB degradation is not obviously changed according to the SEM images (Fig. 2 and S3, ESI†).

Effects of the amount of WO_3 nanoplates, WO_3 morphologies and photoreduction times on the photocatalytic properties of the Ag/AgCl@WO_3 nanostructures

To understand the effect of the amount of WO_3 nanoplates, we synthesized a series of Ag/AgCl@plate–WO_3 photocatalysts with various amounts of WO_3 nanoplates under similar conditions, *i.e.*, the values of $R_{W/(W+Ag)}$ in mole ranging from 18% to 63% (Table S1, ESI†).

Fig. 6a–c shows the typical FE-SEM images of the Ag/AgCl@plate–WO_3 samples with $R_{W/(W+Ag)}$ values of 18% (Fig. 6a), 30% (Fig. 6b) and 63% (Fig. 6c), respectively. As the figures show, the Ag/AgCl nanoparticles with an apparent size of about 100 nm obtained by a 5 min photoreducing reaction are uniformly anchored between the WO_3 nanoplates, forming hierarchically assembled Ag/AgCl@plate–WO_3 composite nanostructures. The Ag/AgCl nanoparticles reduce the possibility of self-agglomeration as the amount of WO_3 nanoplates increases from 18% to 63%, largely enhancing the number of interfacial junctions between the zero-dimensional Ag/AgCl nanoparticles and the two-dimensional WO_3 nanoplates. Fig. 6d shows the typical photodegradation curves of RhB aq. solutions in the presence of Ag/AgCl@plate–WO_3 photocatalysts with various amounts of WO_3 nanoplates under visible-light irradiation ($\lambda \geq 420$ nm). It was found that the amount of WO_3 nanoplates in the Ag/AgCl@plate–WO_3 photocatalysts have an obvious effect on their performance in decomposing RhB dye molecules. Fig. 6e shows a plot of the rate constant k (min^{-1}) as a function of the molar ratio of $R_{W/(W+Ag)}$. The k value increases as the molar ratio of $R_{W/(W+Ag)}$ increases from 0 to about 50%, followed by a sharp reduction when the amount of WO_3 nanoplates increases further.

We also checked the effect of the morphologies of the WO_3 substrates on the photocatalytic performance of the Ag/AgCl@WO_3 photocatalysts. Fig. 7a shows the typical FE-SEM image of WO_3 nanorods obtained by hydrothermally treating a tungsten ammonium aqueous solution at 180 °C for 24 h, and the FE-SEM image of the corresponding Ag/AgCl@rod-WO_3 (AA200rW5) nanostructures is shown in Fig. 7b. One can see

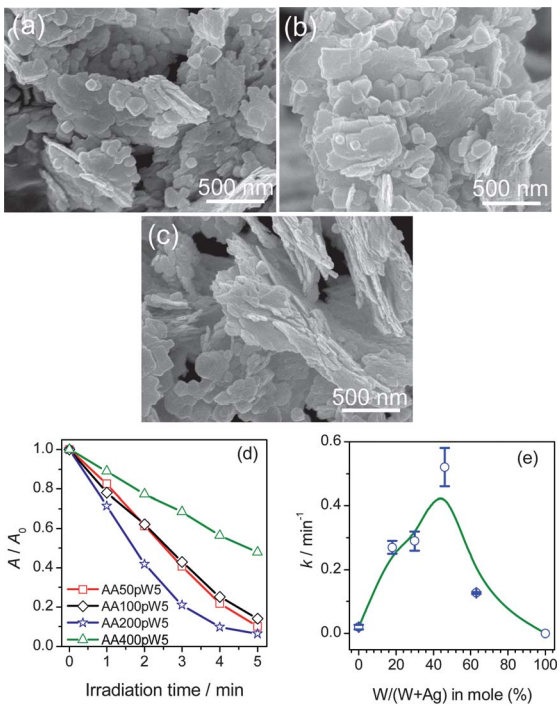

Fig. 6 (a–c) FE-SEM images of Ag/AgCl@plate–WO_3 photocatalysts with various amounts of WO_3 nanoplates: (a) AA50pW5 (18%W), (b) AA100pW5 (30%W) and (c) AA400pW5 (63%W); (d) plots of A/A_0 for RhB aqueous solutions *vs.* the reaction time in the presence of the as-obtained Ag/AgCl@plate–WO_3 photocatalysts with various amounts of WO_3 nanoplates under visible-light irradiation ($\lambda \geq 420$ nm); (e) the effect of the WO_3 nanoplate content on the degradation rates of RhB aqueous solutions under visible-light irradiation ($\lambda \geq 420$ nm).

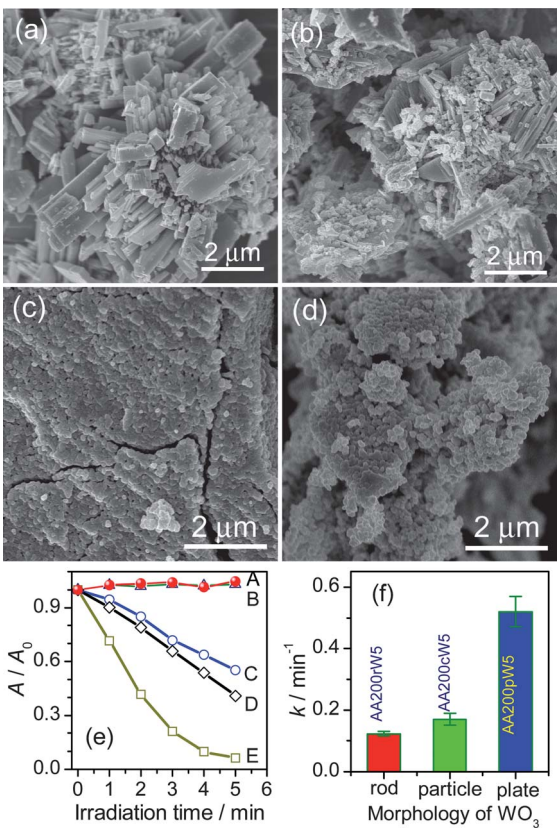

Fig. 7 (a–d) FE-SEM images of (a) WO_3 nanorods and (b) their corresponding Ag/AgCl@rod–WO_3 (AA200rW5), (c) commercially available WO_3 nanoparticles and (d) their corresponding Ag/AgCl@commercial–WO_3 (AA200cW5); (e) plots of A/A_0 for RhB aq. solutions *vs.* the reaction time in the presence of various photocatalysts: (A) commercial WO_3 nanoparticles, (B) WO_3 nanoplates, (C) Ag/AgCl@rod–WO_3 (AA200rW5), (D) Ag/AgCl@commercial–WO_3 (AA200cW5), and Ag/AgCl@plate–WO_3 (AA200pW5) photocatalysts under visible-light irradiation ($\lambda \geq 420$ nm); (f) the comparison of the RhB degradation rates of the Ag/AgCl@WO_3 photocatalysts consisting of WO_3 substrates with various morphologies under visible-light irradiation.

that the Ag/AgCl nanoparticles are dispersed in the void spaces between the WO_3 nanorods. For the purposes of comparison, the commercially available WO_3 nanoparticles (~100 nm) with an agglomeration morphology (Fig. 7c) were also used as the substrates to synthesize Ag/AgCl@commercial-WO_3 (AA200cW5) nanostructures (Fig. 7d) under the same conditions. When comparing Fig. 7c and d, it was found that the combination of Ag/AgCl nanocrystals on the WO_3 nanoparticles improves the dispersibility of the AA200cW5 photocatalyst. Fig. 7e shows the plots of A/A_0 for RhB aq. solutions *vs.* the reaction time in the presence of Ag/AgCl@WO_3 photocatalysts containing WO_3 substrates ($R_{W/(W+Ag)} = 46\%$) with various morphologies (*i.e.*, nanoplates, nanorods and nanoparticles). The performance of the as-obtained Ag/AgCl@rod–WO_3 and Ag/AgCl@commercial–WO_3 is similar, but much lower than that of the Ag/AgCl@plate–WO_3 photocatalyst in photodegrading RhB dyes. As Fig. 7f shows, the rate constant (k) of the Ag/AgCl@plate–WO_3 photocatalyst in degrading RhB is almost three times higher than those of the Ag/AgCl@rod–WO_3 and Ag/AgCl@commercial–WO_3 photocatalysts. A possible explanation could be that the substrate of the WO_3 nanoplates is capable of providing higher surface areas and more interfacial active sites for photocatalysis than those of the WO_3 rods or particles. Actually, the BET surface areas of the Ag/AgCl@plate–WO_3 (AA200pW5) and Ag/AgCl@rod–WO_3 (AA200rW5) photocatalysts are 12.98 $m^2\ g^{-1}$ and 0.93 $m^2\ g^{-1}$, respectively (Fig. S4, ESI†).

In addition, we investigated the effect of photoreduction times during the synthesis of the Ag/AgCl@plate–WO_3 photocatalysts with the same molar ratio of $R_{W/(W+Ag)} = 46\%$ on their photocatalytic performance in visible-light-driven decomposing RhB dye molecules. Fig. 8a shows the plots of A/A_0 for RhB aq. solutions as a function of the irradiation times of visible light in the presence of Ag/AgCl@plate–WO_3 photocatalysts synthesized with various photoreduction times (0–30 min). Fig. 8b gives the comparison results of the rate constant k of the RhB degradation rates under visible-light irradiation of the Ag/AgCl@WO_3 photocatalysts obtained with various photoreduction times. It was found that the Ag/AgCl@plate–WO_3 sample with a photoreduction time of 5 min has the highest photodegradation rate, and the photodegradation rate decreases as the photoreduction time increases from 5 min to 10 min and then up to 30 min, as shown in Fig. 8b. To test whether the photoreduction time is directly proportional to the amount of the metal Ag species generated in the Ag/AgCl@plate–WO_3 photocatalysts, we synthesized Ag/AgCl@plate–WO_3 samples with a longer photoreduction time of 80 min under similar conditions. It is worth noting that there is no obvious increase in the amount of Ag according to the XRD patterns (Fig. S5, ESI†). The present results shown in Fig. 8 and S5† indicate that the most important factor is not the amount of the metal Ag species, but their microstructures (such as sizes and shapes) that influence the photocatalytic performance of the Ag/AgCl@plate–WO_3 samples in decomposing RhB dye molecules. This may relate to the surface plasmon resonance (SPR) effect of metal Ag species, usually influenced by the sizes and shapes of the Ag nanoparticles,[7] but more investigation is required to improve this understanding.

Mechanisms for the photocatalytic performance enhancement of the Ag/AgCl@plate–WO_3 nanostructures

To further understand the mechanism for the remarkably enhanced photocatalytic performance of the Ag/AgCl@plate–WO_3 photocatalysts, we compared the as-obtained Ag/AgCl@plate–WO_3 photocatalyst (AA200pW5) with WO_3 nanoplates, TiO_2 (P25) nanocrystals, Ag/AgCl (AA5) nanocrystals and AgCl@plate–WO_3 (AA200pW0) in decomposing RhB aq. solutions under similar visible-light conditions. The typical results are shown in Fig. 9. One can see that the decreasing order in visible-light-driven photo-decomposing RhB dye molecules of these photocatalysts is Ag/AgCl@plate–WO_3 ≫ AgCl@plate–WO_3 > Ag/AgCl > TiO_2 (P25) > WO_3 nanoplates, and the photocatalytic activity of the Ag/AgCl@plate–WO_3 sample is much higher than those of the separate Ag/AgCl and WO_3 nanoplates.

Fig. 10 shows the typical UV-vis diffuse reflectance spectra of (a) WO_3 nanoplates, (b) AgCl, (c) Ag/AgCl (AA5) and (d) Ag/AgCl@plate–WO_3 (AA200pW5). The absorption edges of the WO_3 nanoplates and AgCl sample obtained here are about 480 nm and 409 nm (Fig. 10a and b). The corresponding energy

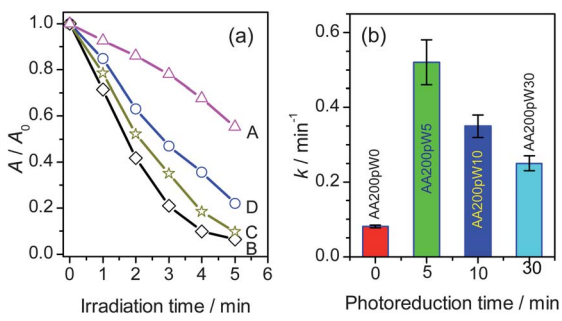

Fig. 8 (a) Plots of A/A_0 for RhB aq. solutions *vs.* the irradiation time of visible light ($\lambda \geq 420$ nm) in the presence of Ag/AgCl@plate–WO_3 photocatalysts with various photoreduction times: (A) 0 min (AA200pW0), (B) 5 min (AA200pW5), (C) 10 min (AA200pW10), and (D) 30 min (AA200pW30); (b) the comparison of the RhB degradation rates of the Ag/AgCl@WO_3 photocatalysts obtained with various photoreduction times under visible-light irradiation ($\lambda \geq 420$ nm).

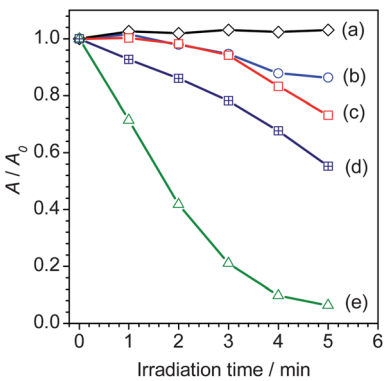

Fig. 9 Plots of A/A_0 for RhB aq. solutions *vs.* the reaction time in the presence of various photocatalysts under visible-light irradiation ($\lambda \geq 420$ nm): (a) WO_3 nanoplates, (b) TiO_2 (P25) nanocrystals, (c) Ag/AgCl (AA5) nanocrystals, (d) AgCl@plate–WO_3 (AA200pW0) and (e) Ag/AgCl@plate–WO_3 (AA200pW5).

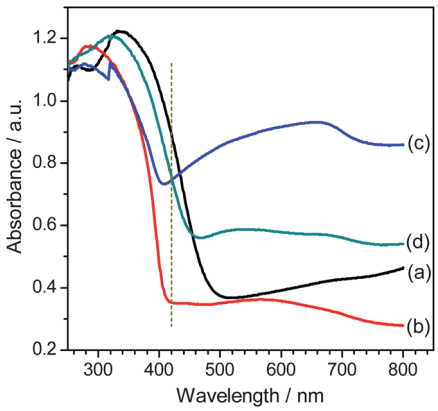

Fig. 10 UV-vis diffuse reflectance spectra of (a) WO_3 nanoplates, (b) AgCl, (c) Ag/AgCl (AA5) and (d) Ag/AgCl@plate–WO_3 (AA200pW5).

band gaps of the WO_3 nanoplates and AgCl sample were determined to be 2.57 eV and 3.03 eV, respectively, according to their plots of $(\alpha h\nu)^{1/2}$ *vs.* $h\nu$ (Fig. S6, ESI†). The sample of Ag/AgCl obtained by photoreducing AgCl under visible light irradiation for 5 min shows a high and wide absorption band in the wavelength range of 420–800 nm (Fig. 10c), and this strong absorption should be attributed to the SPR effect of the Ag species formed *in situ* on the surfaces of the AgCl nanoparticles.[58] The absorbance of the Ag/AgCl@plate–WO_3 is located in the middle of the Ag/AgCl and WO_3 nanoplates (Fig. 10d), and can be thought to be the superimposition of the spectra from Ag/AgCl and WO_3 nanoplates. Considering Fig. 9 and 10, one can easily find that the photocatalytic activity of the Ag/AgCl sample is much lower than that of the Ag/AgCl@plate–WO_3 photocatalyst, though the absorbance of the former is much higher than that of the latter in the experimental wavelength range of $\lambda > 420$ nm. This point indicates that the photocatalytic activity of a photocatalyst is not only relative to its absorption of light, but also other factors, such as the separation efficiency of photogenerated electron–hole pairs, and the number of the effectively active sites for photodegradation.

The remarkably enhanced photocatalytic performance of the Ag/AgCl@plate–WO_3 photocatalysts can be understood from the following aspects. Firstly, the assemblage of Ag/AgCl nanoparticles on the surfaces of the WO_3 nanoplates forms a uniquely hierarchical nanostructure, which provides a high surface area and a large number of interfaces between the Ag/AgCl and WO_3 species. The high surface areas and profuse interfaces are accessible to the outer environment, and provide numerous active sites for the photodegradation of dye molecules. Secondly, the metal Ag clusters formed *in situ* on the semiconductors AgCl and the WO_3 nanocrystals remarkably enhance the absorption in the visible light region because of the surface plasmonic resonance (SPR) effect (Fig. 11a), which photogenerates transient holes that can oxidize the dye molecules.[9,56,59–61] Thirdly, the positively synergistic effects of the coupling of Ag/AgCl and the WO_3 nanocrystals improve the effective separation of the photo-generated electron–hole pairs, and then enhance the photocatalytic performance of the Ag/AgCl@plate–WO_3 photocatalyst.[61] The possible transfer routes of the photo-generated electrons and holes are shown in Fig. 11b, but some details need further investigation.[58–61]

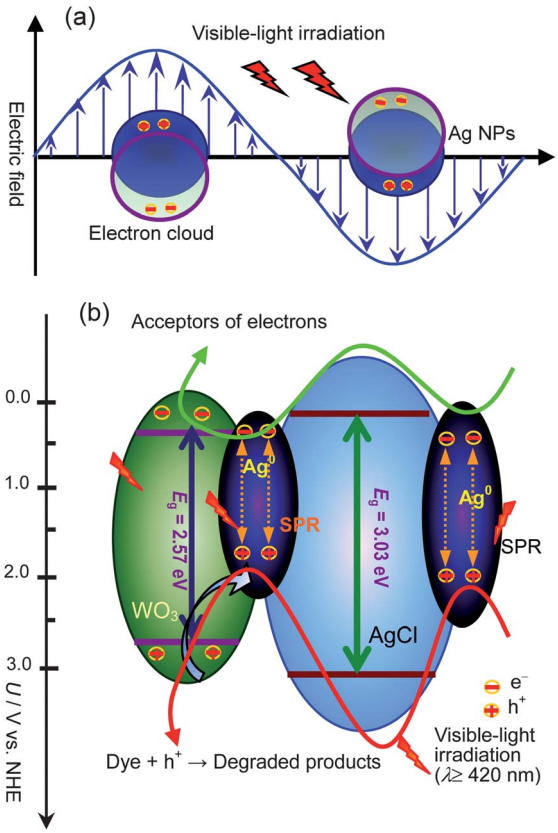

Fig. 11 (a) A schematic for the surface plasmon resonance (SPR) effect of Ag nanoparticles; (b) a schematic of an energy diagram and charge separation in the hierarchical Ag/AgCl@plate–WO_3 photocatalysts.

Conclusions

We have developed a highly efficient visible-light-driven photocatalyst of Ag/AgCl@plate–WO_3 with a hierarchical microstructure by assembling Ag/AgCl nanocrystals on the surfaces of two-dimensional WO_3 nanoplates. The WO_3 nanoplates were synthesized *via* an intercalation and topochemical approach, and the Ag/AgCl@plate–WO_3 photocatalysts were formed through a heterogeneous precipitation process, followed by a photoreduction reaction. The morphologies and contents of the WO_3 substrates, together with the photoreduction times, have appreciable effects on their photocatalytic performance. The Ag/AgCl@plate–WO_3 photocatalyst with a $R_{Ag/(Ag+W)}$ molar ratio of 46% and a photoreduction time of 5 min displayed the highest photocatalytic activity, finishing decomposing a 10 mg L^{-1} RhB aq. solution in 5 min with a rate of $k = 0.52$ min^{-1}. We attribute the enhanced photocatalytic performance of the as-obtained Ag/AgCl@plate–WO_3 photocatalyst to (i) the hierarchical microstructures with high opening surface areas and profuse interfacial active sites, (ii) the enhanced absorption of visible light due to the SPR effects of Ag nanoclusters formed *in situ*, and (iii) the positively synergistic effects of the AgCl and WO_3 substrates in effective separation of photo-generated electrons and holes. Anchoring zero-dimensional functional nanoparticles on two-dimensional nanoplates to construct hierarchical composite nanostructures proposed here open a cost-effective and facile way to achieve highly efficient photocatalysts with promising

applications in environmental purification and energy conversion.

Acknowledgements

This work was supported by the National Natural Science Foundation of China (grant no. 50802090, grant no. 51172211), the China Postdoctoral Science Foundation (grant no. 20090450094, grant no. 201003397), the Foundation for University Young Key Teacher by Henan Province (grant no.2011GGJS-001), and the Advanced Programs of Returned Overseas Researchers of Henan Province (grant no. [2011] 17).

Notes and references

1 X. Chen, S. Shen, L. Guo and S. S. Mao, *Chem. Rev.*, 2010, **110**, 6503–6570.
2 A. Fujishima and K. Honda, *Nature*, 1972, **238**, 37–38.
3 E. Borgarello, J. Kiwi, E. Pelizzetti, M. Visca and M. Grätzel, *Nature*, 1981, **289**, 158–160.
4 C. Ratanatawanate, A. Chyao and K. J. Balkus, *J. Am. Chem. Soc.*, 2011, **133**, 3492–3497.
5 B. Naik, K. M. Parida and C. S. Gopinath, *J. Phys. Chem. C*, 2010, **114**, 19473–19482.
6 R. Abe, H. Takami, N. Murakami and B. Ohtani, *J. Am. Chem. Soc.*, 2008, **130**, 7780–7781.
7 (*a*) W. A. Murray and W. L. Barnes, *Adv. Mater.*, 2007, **19**, 3771–3782; (*b*) E. M. Larsson, C. Langhammer, I. Zoric and B. Kasemo, *Science*, 2009, **326**, 1091–1094; (*c*) J. Yu, H. Tao and B. Cheng, *ChemPhysChem*, 2010, **11**, 1617–1618.
8 C. H. An, S. N. Peng and Y. G. Sun, *Adv. Mater.*, 2010, **22**, 2570–2574.
9 D. Tsukamoto, Y. Shiraishi, Y. Sugano, S. Ichikawa, S. Tanaka and T. Hirai, *J. Am. Chem. Soc.*, 2012, **134**, 6309–6315.
10 Z. H. Xu, J. G. Yu and G. Liu, *Electrochem. Commun.*, 2011, **13**, 1260–1263.
11 Z. K. Zheng, B. B. Huang, X. Y. Qin, X. Y. Zhang, Y. Dai and M. H. Whangbo, *J. Mater. Chem.*, 2011, **21**, 9079–9087.
12 D. B. Ingram and S. Linic, *J. Am. Chem. Soc.*, 2011, **133**, 5202–5205.
13 M. Zhu, P. Chen and M. Liu, *J. Mater. Chem.*, 2011, **21**, 16413–16419.
14 H. Xu, H. Li, J. Xia, S. Yin, Z. Luo, L. Liu and L. Xu, *ACS Appl. Mater. Interfaces*, 2011, **3**, 22–29.
15 Z. Lou, B. Huang, P. Wang, Z. Wang, X. Qin, X. Zhang, H. Cheng, Z. Zheng and Y. Dai, *Dalton Trans.*, 2011, **40**, 4104–4110.
16 J. Jiang and L. Zhang, *Chem.–Eur. J.*, 2011, **17**, 3710–3717.
17 L. Han, P. Wang, C. Zhu, Y. Zhai and S. Dong, *Nanoscale*, 2011, **3**, 2931–2935.
18 P. Wang, B. Huang, Q. Zhang, X. Zhang, X. Qin, Y. Dai, J. Zhan, J. Yu, H. Liu and Z. Lou, *Chem.–Eur. J.*, 2010, **16**, 10042–10047.
19 L. Kuai, B. Geng, X. Chen, Y. Zhao and Y. Luo, *Langmuir*, 2010, **26**, 18723–18727.
20 S. M. Sun, W. Z. Wang, L. Zhang, M. Shang and L. Wang, *Catal. Commun.*, 2009, **11**, 290–293.
21 (*a*) H. Kim, J. Kim, W. Kim and W. Choi, *J. Phys. Chem. C*, 2011, **115**, 9797–9805; (*b*) M. R. Elahifard, S. Rahimnejad, S. Haghighi and M. R. Gholami, *J. Am. Chem. Soc.*, 2007, **129**, 9552–9553.
22 (*a*) J. Yu, L. Zhang, B. Cheng and Y. Su, *J. Phys. Chem. C*, 2007, **111**, 10582–10589; (*b*) J. Yu, W. Wang and B. Cheng, *Chem.–Asian J.*, 2010, **5**, 2499–2506.
23 H. Li, X. He, Z. Kang, H. Huang, Y. Liu, J. Liu, S. Lian, C. H. A. Tsang, X. Yang and S.-T. Lee, *Angew. Chem., Int. Ed.*, 2010, **49**, 4430–4434.
24 W. Yao, B. Zhang, C. Huang, C. Ma, X. Song and Q. Xu, *J. Mater. Chem.*, 2012, **22**, 4050–4055.
25 D. Wang, Y. Duan, Q. Luo, X. Li, J. An, L. Bao and L. Shi, *J. Mater. Chem.*, 2012, **22**, 4847–4854.
26 G. Tian, Y. Chen, H.-L. Bao, X. Meng, K. Pan, W. Zhou, C. Tian, J.-Q. Wang and H. Fu, *J. Mater. Chem.*, 2012, **22**, 2081–2088.
27 Y. Zhang, Z.-R. Tang, X. Fu and Y.-J. Xu, *Appl. Catal., B*, 2011, **106**, 445–452.
28 C. Hu, Y. Q. Lan, J. H. Qu, X. X. Hu and A. M. Wang, *J. Phys. Chem. B*, 2006, **110**, 4066–4072.
29 Y. Hou, X. Li, Q. Zhao, X. Quan and G. Chen, *J. Mater. Chem.*, 2011, **21**, 18067–18076.
30 M. Zhu, P. Chen and M. Liu, *Langmuir*, 2012, **28**, 3385–3390.
31 M. Zhu, P. Chen and M. Liu, *ACS Nano*, 2011, **5**, 4529–4536.
32 Y. Bi, S. Ouyang, J. Cao and J. Ye, *Phys. Chem. Chem. Phys.*, 2011, **13**, 10071–10075.
33 X. Wang, S. Li, H. Yu and J. Yu, *J. Mol. Catal. A: Chem.*, 2011, **334**, 52–59.
34 C. Jing, X. Benyan, L. Bangde, L. Haili and C. Shifu, *Appl. Surf. Sci.*, 2011, **257**, 6644–7089.
35 J. F. Guo, B. W. Ma, A. Y. Yin, K. N. Fan and W. L. Dai, *Appl. Catal., B*, 2011, **101**, 580–586.
36 H. Cheng, B. Huang, P. Wang, Z. Wang, Z. Lou, J. Wang, X. Qin, X. Zhang and Y. Dai, *Chem. Commun.*, 2011, **47**, 7054–7056.
37 C. Hu, T. W. Peng, X. X. Hu, Y. L. Nie, X. F. Zhou, J. H. Qu and H. He, *J. Am. Chem. Soc.*, 2010, **132**, 857–862.
38 Z. Zhou, M. Long, W. Cai and J. Cai, *J. Mol. Catal. A: Chem.*, 2012, **353–354**, 22–28.
39 J.-F. Guo, B. Ma, A. Yin, K. Fan and W.-L. Dai, *J. Hazard. Mater.*, 2012, **211–212**, 77–82.
40 C. An, X. Ming, J. Wang and S. Wang, *J. Mater. Chem.*, 2012, **22**, 5171–5176.
41 H. Zhang, X. Fan, X. Quan, S. Chen and H. Yu, *Environ. Sci. Technol.*, 2011, **45**, 5731–5736.
42 Y. Xua, H. Xu, H. Li, J. Xia, C. Liu and L. Liu, *J. Alloys Compd.*, 2011, **509**, 3286–3292.
43 W. Xiong, Q. Zhao, X. Li and D. Zhang, *Catal. Commun.*, 2011, **16**, 229–233.
44 Y. Tang, V. P. Subramaniam, T. H. Lau, Y. Lai, D. Gong, P. D. Kanhere, Y. H. Cheng, Z. Chen and Z. Dong, *Appl. Catal., B*, 2011, **106**, 577–585.
45 J. Yu, G. Dai and B. Huang, *J. Phys. Chem. C*, 2009, **113**, 16394–16401.
46 J. Lei, W. Wang, M. Song, B. Dong, Z. Li, C. Wang and L. Li, *React. Funct. Polym.*, 2011, **71**, 1071–1076.
47 T. Arai, M. Yanagida, Y. Konishi, Y. Iwasaki, H. Sugihara and K. Sayama, *J. Phys. Chem. C*, 2007, **111**, 7574–7577.
48 J. Cao, B. Luo, H. Lin and S. Chen, *J. Hazard. Mater.*, 2011, **190**, 700–706.
49 J. Cao, B. Luo, H. Lin and S. Chen, *J. Mol. Catal. A: Chem.*, 2011, **344**, 138–144.
50 P. Wang, B. Huang, X. Qin, X. Zhang, Y. Dai and M.-H. Whangbo, *Inorg. Chem.*, 2009, **48**, 10697–10702.
51 (*a*) S. Sun, X. Chang, L. Dong, Y. Zhang, Z. Li and Y. Qiu, *J. Solid State Chem.*, 2011, **184**, 2190–2195; (*b*) B. Ma, J. Guo, W.-L. Dai and K. Fan, *Appl. Catal., B*, 2012, **123–124**, 193–199.
52 D. Chen and Y. Sugahara, *Chem. Mater.*, 2007, **19**, 1808–1815.
53 D. Chen, T. Li, L. Yin, X. Hou, X. Yu, Y. Zhang, B. Fan, H. Wang, X. Li, R. Zhang, T. Hou, H. Lu, H. Xu, J. Sun and L. Gao, *Mater. Chem. Phys.*, 2011, **125**, 838–845.
54 D. Chen, L. Gao, A. Yasumori, K. Kuroda and Y. Sugahara, *Small*, 2008, **4**, 1813–1822.
55 D. Chen, X. Hou, H. Wen, Y. Wang, H. Wang, X. Li, R. Zhang, H. Lu, H. Xu, S. Guan, J. Sun and L. Gao, *Nanotechnology*, 2010, **21**, 035501.
56 D. Chen, S. H. Yoo, Q. Huang, G. Ali and S. O. Cho, *Chem.–Eur. J.*, 2012, **18**, 5192–5200.
57 S. Glaus and G. Calzaferri, *Photochem.Photobiol. Sci.*, 2003, **2**, 398–401.
58 (*a*) Q. Xiang, J. Yu, B. Cheng and H. C. Ong, *Chem.–Asian J.*, 2010, **5**, 1466–1474; (*b*) E. Kazuma, T. Yamaguchi, N. Sakai and T. Tatsuma, *Nanoscale*, 2011, **3**, 3641–3645; (*c*) T. Wu, S. Liu, Y. Luo, W. Lu, L. Wang and X. Sun, *Nanoscale*, 2011, **3**, 2142–2144.
59 M. R. Jones, K. D. Osberg, R. J. Macfarlane, M. R. Langille and C. A. Mirkin, *Chem. Rev.*, 2011, **111**, 3736–3827.
60 (*a*) J. Lan, X. Zhou, G. Liu, J. Yu, J. Zhang, L. Zhi and G. Nie, *Nanoscale*, 2011, **3**, 5161–5167; (*b*) J. Zhou, Y. Cheng and J. Yu, *J. Photochem. Photobiol., A*, 2011, **223**, 82–87.
61 Y. Tian and T. Tatsuma, *J. Am. Chem. Soc.*, 2005, **127**, 7632–7637.